# A refined Morphological Representative Pattern approach to the behavior of polydisperse highly-filled inclusion-matrix composites

Thai Son Vu, Bao-Viet Tran, Hoang-Quan Nguyen, Xavier Chateau

# A refined Morphological Representative Pattern approach to the behavior of polydisperse highly-filled inclusion-matrix composites

Thai-Son Vu[a], Bao-Viet Tran[b,*], Hoang-Quan Nguyen[b], Xavier Chateau[c]

[a]*Division of Bridge and Tunnel Engineering, Hanoi University of Civil Engineering, Hanoi, Vietnam*
[b]*Research and Application Center for Technology in Civil Engineering (RACE), Construction Engineering Faculty, University of Transport and Communications, 3 Cau Giay, Lang Thuong, Dong Da, Hanoi, Vietnam*
[c]*Navier, Ecole des Ponts, Univ Gustave Eiffel, CNRS, Marne-la-Vallée, France*

**Abstract**

This study presents a new micromechanical model that is simple, explicit, and directly applicable for broad engineering applications to predict the effective elastic moduli of very high-contrast component property composites containing high concentrations of particles. The approach is based on the Morphological Representative Pattern scheme, where the first pattern comprises a spherical fictitious inclusion embedded in an infinite effective homogeneous medium with physical properties of the matrix, while the others correspond to the classical three-phase generalized self-consistent problem. Instead of using the mean distance between particles, as addressed in existing literature, the volume fraction of patterns is calculated based on the maximum packing fraction estimated from the packing model. This approach shows perfect coherence with experimental data for benchmark examples of effective properties of suspensions of monodisperse particles in an elastic matrix and porous materials. Furthermore, a refined version of the model is proposed, which includes a free parameter representing the shape of the fictitious inclusion to evaluate the polydisperse effect on the overall properties of these materials.

*Keywords:* maximum packing effect, micromechanical model, generalized self-consistent, polydispersity, multicomponent, yield stress fluid, porous media

## 1. Introduction

Over the past few decades, the overall behavior of composite materials has been extensively studied due to their practical applications and theoretical importance. The effective medium approach is a suitable method for this research as it allows for the consideration of the composition and microstructure of composites, such as the orientations, shapes, volume fractions, and spatial distribution of inclusions, as well as the behavior of constituents. Various effective medium micromechanical models can be found in mechanical handbooks

*Corresponding author, *E-mail address*: viettb@utc.edu.vn

and reviews [1, 2, 3, 4]. Almost all approximations, such as dilute, self-consistent [5, 6], differential [7, 8], and Mori-Tanaka [9] schemes, are based on the classical analytical Eshelby solution [10] for ellipsoidal inclusions embedded in an infinite homogeneous domain, where the stress and strain fields within the inclusions are homogeneous. However, classical models have two disadvantages. Firstly, they are unable to accurately account for the size effect or crowding phenomena. Secondly, classical models are incapable of accurately predicting the overall elastic modulus of composites with a volume fraction of inclusion phases near the maximum packing fraction, particularly for high-contrast-component-property composites, such as suspensions of rigid particles in yield stress fluids, porous materials, or inclusion-matrix composite materials that differ in component stiffness. For example, a random suspension of rigid spheres in an elastic matrix near the maximum packing fraction has been experimentally observed to diverge at a solid volume fraction of approximately 60% for monodisperse particles [11] and even greater for polydisperse particles [12], while the self-consistent estimate for the same material tends towards infinity at a rigid volume fraction close to 40%. Similar deficiencies have been reported when these schemes are used to predict the overall properties of porous media [4]. Consequently, the estimates developed based on Eshelby's scheme for these materials often fail to accurately predict their effective properties, which limits their practical application.

Numerous modified classical micromechanical models have been proposed to overcome the challenge at hand. Norris [13] introduced the generalized differential approximation (GDA), which assumes that a part of the matrix domain cannot be replaced by the inclusion phase during the incremental process of the differential scheme. This region is modeled as fictitious spherical inclusions with matrix material properties. By reducing the maximum allowable volume fraction for the inclusion phase to the remaining matrix domain, different values of the maximum volume fraction can be considered. Phan-Thien and Pham [14, 15] utilized the GDA scheme to estimate the thermal conductivity and effective viscosity of spheroids suspension. More recently, Markov [16, 17] applied GDA to compute the effective electric conductivity of a two-dimensional percolating medium. Although Markov demonstrated the accurate prediction of the experimental electrical conductivity of biphasic materials using the GDA scheme, this approach cannot be generalized to include the particle packing model to predict the maximum packing fraction of polydisperse particles, the reason being that it lacks any length scale that can be linked to particle size or interparticle distance. Shashidhar et al. [18] proposed a modified version of the generalized self-consistent approximation model [19] with two adjustable parameters: the percolation threshold and the maximum packing fraction of the inclusions. However, it is difficult to generalize the model's applicability since the homogenization scheme used to estimate the material's overall properties is not rigorously linked to the percolation model [20], even if the model accurately fits experimental data for asphalt mastic.

Several modified versions of classical Eshelby-based models have been proposed by Pham et al. [21, 22], Nguyen et al. [23], Timothy et al. [24], and Tran et al. [25, 26]. These models contain free parameters, such as properties of reference medium in [21, 23, 25, 26], and several cascade levels in [24], that can be adjusted to successfully simulate the properties of materials with different microstructures. However, as these models do not rely on homogenization schemes that describe observable or measurable microstructure properties, their generalization to many different materials is limited. Nevertheless, this adaptive strategy can be useful to account for particular cases and improve the effectiveness and flexibility of the models.

Beginning with the pioneering work of Hashin [27], the Morphological Representative Pattern (MRP) approach [28, 29, 30, 31, 32] aims to incorporate microstructure information by considering the heterogeneous material as several sets of identical composite inclusions (the patterns), where the spatial distribution of centers can be explained by statistical information. Unlike classical mechanical phases that differ based on their mechanical properties, the considered patterns act as morphological phases, providing access to individual particles or domains with specific attributes, such as size and surface area. This allows the MRP approach to more effectively predict the effective behavior of multiphase materials by incorporating pertinent information about the geometric characteristics of their constituent phases. Marcadon et al. [33] used the MRP approach to account for packing and size effect phenomena in isotropic elastic composites with isotropically distributed monodisperse spherical particles. They suggested that some geometric pattern parameters may be correlated with the mean distance between nearest-neighbor particles, estimated and bounded in [34]. Although the paper [33] proposed an interesting approach to account for the size and crowding effects in a particular composite, the authors did not validate their hypotheses by comparing their model's predictions with experimental data.

Majewski et al. expanded Marcadon's model by validating its theoretical predictions with numerical data through finite element computational homogenization for both linear [35, 36] and nonlinear [37] problems. However, the lack of detailed calculations involving geometric information in the pattern makes the packing parameter function more as a fitting parameter rather than a physically determinable quantity. Furthermore, the differentiation between the isotropic configuration employed in the analytical approach and the anisotropic configuration utilized in the periodic homogenization technique, along with the absence of a comparison between the model's predictions and empirical findings, continue to be ongoing points of contention in this field.

This brief review suggests that the validation of a general micromechanical approach that can accurately predict the effective elastic moduli of very high-contrast component property composites with high concentrations of particles needs to be carefully considered and evaluated. To simplify and make the paper relevant to observable empirical applications,

we have limited the scope to the domain of isotropic elastic composites with isotropically distributed spherical particles. We first reconstruct the MRP approach in Sections 2 and 3. Next, we compare the model's predictions to the available experimental data for monodisperse/polydisperse matrix-inclusion composites or specific porous materials in Section 4. This comparison enables us to demonstrate that the shell thickness of patterns defined in the MRP approach is not equivalent to the mean distance between nearest-neighbor particles estimated and bounded in [34]. Instead, it can be estimated from a simple geometric approximation related to the maximum packing fraction of the inclusions. Unfortunately, this model is invalid for polydisperse inclusion-matrix composite materials. Hence, we propose a more comprehensive and adaptable model in Section 5, which takes into account the shape effect of fictitious inclusions. This new model serves to demonstrate the possible application of the MRP approach in the case of polydisperse inclusion-matrix composite materials.

## 2. Review of effective medium approximations

We begin by considering the elastic isotropic problem for a composite material composed of $n$ inclusion phases, each with a stiffness fourth order tensor $\mathbb{C}_i$ (comprising bulk modulus $K_i$ and shear modulus $\mu_i$), volume fraction $\phi_i$ ($i = 1..n$), a specific ellipsoidal shape, and a specific orientation in a matrix with a stiffness fourth order tensor $\mathbb{C}_m$ ($K_m$, $\mu_m$) and volume fraction $\phi_m$. Eshelby's work [10] established that a single ellipsoidal inclusion embedded in an unbounded matrix under remote homogeneous deformation is also in homogeneous deformation proportional to the matrix's remote deformation with a proportional coefficient known as the Eshelby fourth order tensor $\mathbb{S}_E$. If the inclusions are distributed non-preferably (i.e., randomly) in the space, the resulting composite is isotropic. Asymptotically exact solutions for the effective moduli of a dilute suspension of randomly oriented, well-separated ellipsoidal inclusions (resulting in an isotropic effective medium) are given by [3]:

$$K^e = K_m + \sum_{i=1}^{n} \phi_i (K_i - K_m) A_i^s \tag{1}$$

$$\mu^e = \mu_m + \sum_{i=1}^{n} \phi_i (\mu_i - \mu_m) A_i^d \tag{2}$$

where $A_i^s, A_i^d$ are the shape functions of the inclusion phase $i$, which correspond respectively to the spherical and deviatoric components of the strain localization fourth-order tensor $\mathbb{A}_i$. These shape functions can be calculated using the Eshelby solution for the geometric property of inclusions. The expressions for $A_i^s$ and $A_i^d$ will be provided in Section 5 and the Appendix.

The differential approximation (DA) is constructed from the differential scheme process and the dilute solution. At each step of the procedure, we add proportionally infinitesimal volume amounts $\phi_i \Delta t$ ($\Delta t \ll 1$) of randomly oriented inclusions into the already constructed

composite of the previous step, which contains volume fractions $\phi_i t$ of the inclusion phases ($0 < t < 1$). The DA for the effective elastic moduli of the (n+1)-component matrix composite is the solution $K^e = K(1)$, $\mu^e = \mu(1)$ of coupled differential equations:

$$\frac{dK}{dt} = \frac{1}{1-\phi t}\sum_{i=1}^{n}\phi_i(K_i - K)A_i^s, \tag{3}$$

$$\frac{d\mu}{dt} = \frac{1}{1-\phi t}\sum_{i=1}^{n}\phi_i(\mu_i - \mu)A_i^d \tag{4}$$

with

$$K(0) = K_m, \qquad \mu(0) = \mu_m, \qquad 0 \le t \le 1, \qquad \phi = \sum_{i=1}^{n}\phi_i. \tag{5}$$

By eliminating the matrix phase $m$ from equations (3, 4), the volume fraction of the inclusions becomes $\phi = 1$, and the multiplier $1/(1-\phi t)$ tends towards infinity at the end of the process. This implies that the sums $\sum_{i=1}^{n}\phi_i(K_i - K)A_i^s$ and $\sum_{i=1}^{n}\phi_i(\mu_i - \mu)A_i^d$ tend towards zero since $K$ and $\mu$ must be finite. This approach is known as the self-consistent approximation (SCA) for the n-component mixture of particulates, which is the solution of the self-consistent equations:

$$\sum_{i=1}^{n}\phi_i(K_i - K^e)A_i^s = 0, \tag{6}$$

$$\sum_{i=1}^{n}\phi_i(\mu_i - \mu^e)A_i^d = 0. \tag{7}$$

In this paper, we explore further applications of the coupled self-consistent equations (6, 7) that always obey the Hashin–Shtrikman bounds (HSB), which are the best mathematical bounds based on the component properties and volume content of composites [3]:

$$\mathrm{HSL} = P_K(\mu_{min}) \le K^e \le P_K(\mu_{max}) = \mathrm{HSU} \tag{8}$$

$$\mathrm{HSL} = P_\mu(K_{min}, \mu_{min}) \le \mu^e \le P_\mu(K_{max}, \mu_{max}) = \mathrm{HSU} \tag{9}$$

with

$$K_{min} = \min\{K_m, K_i\}, \qquad K_{max} = \max\{K_m, K_i\}, \tag{10}$$

$$\mu_{min} = \min\{\mu_m, \mu_i\}, \qquad \mu_{max} = \max\{\mu_m, \mu_i\}, \tag{11}$$

where

$$P_K(\mu) = \left( \frac{\phi_m}{K_m + K_*(\mu)} + \sum_{i=1}^{n} \frac{\phi_i}{K_i + K_*(\mu)} \right)^{-1} - K_*(\mu), \tag{12}$$

$$P_\mu(K,\mu) = \left( \frac{\phi_m}{\mu_m + \mu_*(K,\mu)} + \sum_{i=1}^{n} \frac{\phi_i}{\mu_i + \mu_*(K,\mu)} \right)^{-1} - \mu_*(K,\mu), \tag{13}$$

with

$$K_*(\mu) = \frac{4}{3}\mu, \;\; \mu_*(K,\mu) = \frac{9K + 8\mu}{6K + 12\mu}\mu. \tag{14}$$

## 3. The morphological representative pattern approach with maximum packing effect

### *3.1. The basic MRP self-consistent equations*

In this section, we explore the basic configuration and formulas of the MRP approach. We begin by focusing on a simple situation where a linear isotropic composite material is composed of a unique inclusion phase of spherical form embedded in a solid matrix. For this configuration, we consider two spherical patterns (see Figure 1 with $i = 1$). The first pattern corresponds to a fictitious homogeneous sphere with the property of the matrix $(K_m, \mu_m)$ and a volume fraction $c_0$. We investigate the packing effect based on the role of this fictitious sphere. The second pattern consists of a coated sphere with a spherical core made of the inclusion material (radius $R_i^1$, volume fraction $f_i$, elastic shear modulus $\mu_i$, bulk modulus $K_i$) and a spherical shell made of the matrix material (radius $R_i^2$, elastic shear modulus $\mu_m$, bulk modulus $K_m$). Let $c_i$ denote the volume fraction of the second pattern, which is given by $c_i = 1 - c_0$ (only for the two-phase composites where $i = 1$). We denote by $\phi_i$ the volume fraction of the inclusion phase:

$$f_i = \frac{\phi_i}{c_i} = \left( \frac{R_i^1}{R_i^2} \right)^3. \tag{15}$$

We assume that the two patterns are embedded in an Effective Equivalent Medium with effective properties having elastic moduli $\mu^e$ and $K^e$. By applying the self-consistent equations (6, 7) for this configuration, the effective elastic moduli of the material are the solution of

$$c_0(K_m - K^e)A_0^s + c_i f_i (K_i - K^e)A_i^{1s} + c_i(1 - f_i)(K_m - K^e)A_i^{2s} = 0, \tag{16}$$

$$c_0(\mu_m - \mu^e)A_0^d + c_i f_i (\mu_i - \mu^e)A_i^{1d} + c_i(1 - f_i)(\mu_m - \mu^e)A_i^{2d} = 0. \tag{17}$$

The coupled equations (16, 17) present the 2 patterns MRP self-consistent approach for a two-phase matrix-inclusion isotropic composite made of linear elastic isotropic materials (noted as the 2 patterns MRP approach).

The coefficients $A$ are the shape functions for dilute problems that can be calculated based on the configuration of the patterns. Specifically, $A_i^{1s}$, $A_i^{1d}$, $A_i^{2s}$, and $A_i^{2d}$ represent the spherical (superscript "s") and deviatoric (superscript "d") coefficients of the average strain localization tensors for the spherical inclusion (superscript "1") and the coated spherical matrix shell (superscript "2") in pattern $i$. The calculation of these four coefficients can be found in Appendix A and the details are presented in [33, 38]. The coefficients $A_0^s$ and $A_0^d$ represent the spherical and deviatoric coefficients of the average strain localization tensor for the fictitious matrix inclusion pattern in the effective infinite medium. They have the respective expressions of $A_i^{2s}$ and $A_i^{2d}$ when $f_i \to 0$. Equation (16) is linear with respect to $K^e$ and can be solved to compute $K^e$ as a function of $\mu^e$, $\mu_i$, $\mu_m$, $K_i$, $K_m$, $\phi = \phi_i$, and $c_i$. By substituting this solution into equation (17), we obtain a degree 5 polynomial in $\mu^e$. This polynomial has only one real root between $\mu_i$ and $\mu_m$ that satisfies $c_i \in [0, 1]$ and $\phi \in [0, c_i]$.

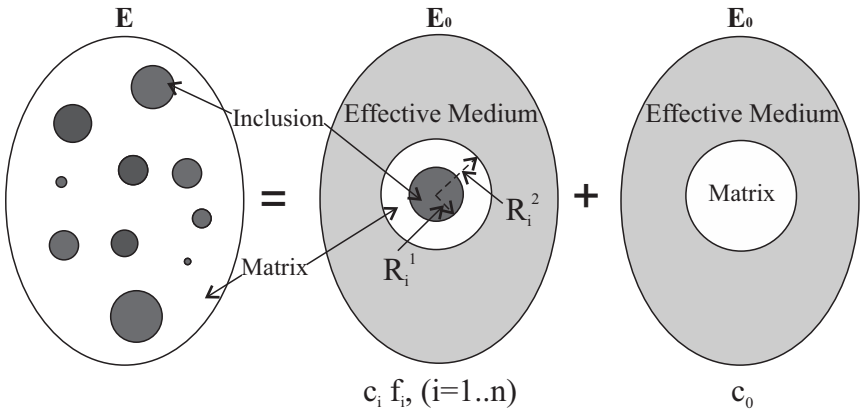


Figure 1: The $(n + 1)$ patterns MRP approach.

Figure 2 shows the overall estimate of the shear elastic modulus for a material composed of rigid spherical particles dispersed in an incompressible elastic matrix, as a function of $\phi$ for different values of $c_i$. Additionally, Figure 2 displays the Hashin-Shtrikman lower bound (HSL) which coincides with both the Mori-Tanaka approach (MTA), and the self-consistent approach (SCA). It is worth noting that the MRP estimate is always greater than the Hashin-Shtrikman lower bound, regardless of the inclusion volume fraction or the composite pattern fraction (the Hashin-Shtrikman upper bound is infinite in this case). Furthermore, the 2 patterns MRP approach tends towards the self-consistent approach as $\phi$ approaches $c_i$ for $c_i < 0.4$, and approaches infinity as $\phi$ approaches $c_i$ for $c_i \geq 0.4$. This result is expected since the 2 patterns MRP approach is identical to the self-consistent approach when $\phi = c_i$. Similarly, the classical Christensen and Lo three-phase model [19] is obtained by setting $c_i = 1$ in the 2 patterns MRP approach.

In the case of an isotropic porous material with an incompressible linear elastic matrix, we set $\mu_i = K_i = 0$ and $K_m = \infty$ in equations (16, 17). The MRP approach for the homogeneous shear modulus is plotted in Figure 3 as a function of porosity for several values

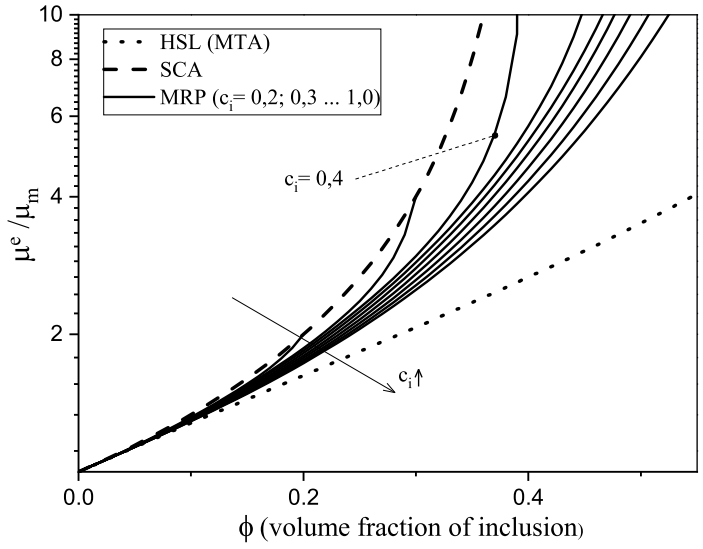


Figure 2: Dimensionless overall elastic shear modulus of a dispersion of rigid spherical inclusions in an isotropic incompressible matrix. The solid lines represent the 2 patterns MRP approach for $c_i$ values ranging from 0.2 to 1.0. The Hashin-Shtrikman lower bound (HSL), which is equivalent to the Mori-Tanaka approach (MTA), is represented by the dotted line. The self-consistent approach (SCA) is shown as a dashed curve.

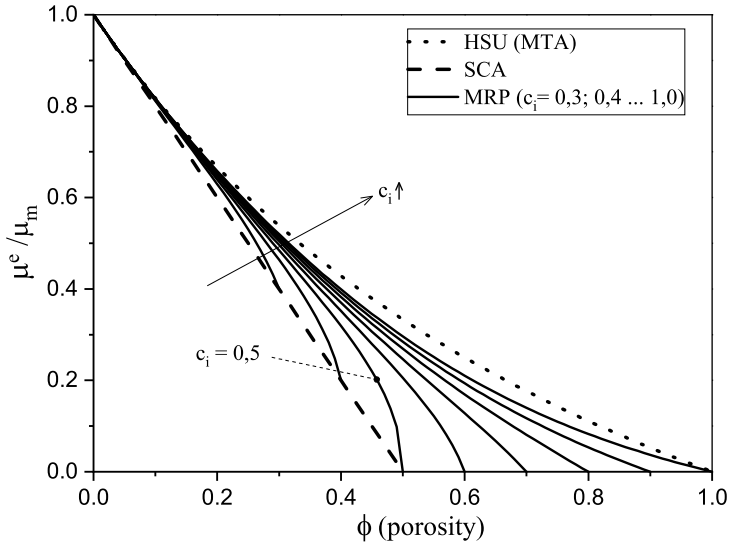


Figure 3: Dimensionless overall elastic shear modulus of dispersion of spherical pores in an isotropic incompressible matrix: The 2 patterns MRP approach for $c_i$ values ranging from 0.3 to 1.0 present as solid lines; Hashin-Shtrikman upper bound (HSU), which is equivalent to the Mori-Tanaka approach (MTA), is represented by the dotted line; the self-consistent approach (SCA) is shown as a dashed curve.

of $c_i$. The Hashin-Shtrikman upper bound (HSU), with the Hashin-Shtrikman lower bound being zero, and the self-consistent approach are also plotted in Figure 3 for comparison. The 2 patterns MRP approach is always lower than the Hashin-Shtrikman upper bound for values

of $c_i \in [0,1]$ and $\phi \in [0, c_i]$. As with rigid inclusion-matrix composites, the 2 patterns MRP approach tends towards the self-consistent approach when $c_i$ is strictly less than 0.5 and towards zero for $c_i \in [0.5, 1]$, for the same reasons mentioned earlier.

It is worth noting that similar trends were observed in [33] for the 2 patterns MRP approach when the two phases behave elastically. The predictions of the classical self-consistent approach are recovered when $\phi$ equals $c_i$ (refer to Figure 3 in [33]) for completeness.

### *3.2. Geometric approximation*

As mentioned in Section 1, the parameter $c_i$ plays a crucial role in the effectiveness of the model. Firstly, we aim to verify the assumption proposed in previous studies [33, 35] that $c_i$ can be calculated from the mean distance between particles. For a suspension of monodisperse rigid particles dispersed in various matrices, the mean distance between nearest-neighbor particles can be expressed as given in [34]:

$$\frac{R_i^2}{R_i^1} = \overline{\lambda} \leq \begin{cases} 1 + \frac{1}{24}\frac{(1-\phi)^3}{\phi\,(1-1/2\,\phi)} & : \quad \phi < 0,49, \\ \\ 1 + \frac{(1-0,49)^3(\phi^M-\phi)}{24\phi(1-0,49/2)(\phi^M-0,49)} & : \quad \phi \geq 0,49. \end{cases} \tag{18}$$

Here, we note that $\phi^M$ represents the maximum packing density of inclusions. Equation (15) shows that:

$$c_i = \phi_i \overline{\lambda}^3 \qquad , \qquad c_0 = 1 - c_i \qquad \text{and} \qquad f_i = 1/\overline{\lambda}^3. \tag{19}$$

By combining the geometric relationships (18, 19) with the coupled self-consistent equations (16, 17), we can derive the MRP estimate for the particulate composite. Here, the volume fraction of patterns is defined by the mean distance between particles.

However, the trends observed in Figs. 2 and 3 suggest a simple geometric approximation where the pattern volume fraction $c_i$ represents the maximum packing fraction of an inclusion-matrix composite or a porous material. If we assume this, the geometric relationships of the model can be expressed in simple forms:

$$c_i = \phi^M, \qquad c_0 = 1 - \phi^M, \qquad f_i = \frac{\phi_i}{\phi^M} \qquad \text{and} \qquad \frac{R_i^2}{R_i^1} = \left(\frac{\phi^M}{\phi_i}\right)^{(1/3)} \tag{20}$$

Figure 4 displays the difference between the two geometric approximations. The dashed curve depicts the upper bound of the $R_i^2/R_i^1$ ratio, as determined by equation (18), while the solid line represents the simple approximation (20). Because of the large difference between these two geometric approximations, and the fact that the MRP method is constructed based on assumptions about configuration and spatial distribution of fictitious patterns, evaluating the effectiveness of this approach is a critical point of the research topic. This will be further explicated in Section 4, which will compare the method with validated experimental results.

By combining equations (16), (17), and (20), we obtain the coupled self-consistent formulas of the 2 patterns MRP approach, denoted as MRPM, which account for the maximum packing effect in the effective elasticity of matrix-inclusion materials with random spherical inclusions.

$$(1-\phi^M)(K_m-K^e)A_0^s+\phi_i(K_i-K^e)A_i^{1s}+(\phi^M-\phi_i)(K_m-K^e)A_i^{2s}=0, \tag{21}$$

$$(1-\phi^M)(\mu_m-\mu^e)A_0^d+\phi_i(\mu_i-\mu^e)A_i^{1d}+(\phi^M-\phi_i)(\mu_m-\mu^e)A_i^{2d}=0. \tag{22}$$

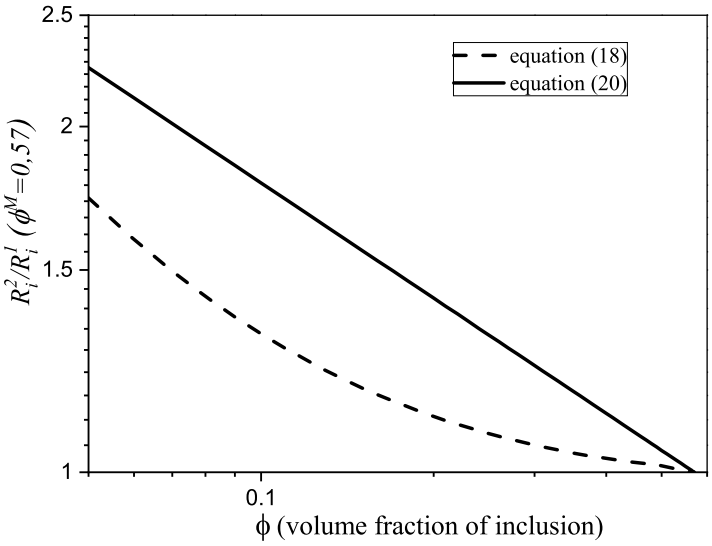


Figure 4: $R_i^1/R_i^2$ ratio defined by the mean distance between the particles (dashed curve) and by the simple geometric approximation (solid line).

An advantage of the simple geometric approximation from equation (20) is that this approximation method easily allows for extending the results from eqs. (21-22) in the case of a multiphase material. Specifically, we consider a multiphase matrix-based composite material consisting of $n$ randomly distributed spherical phase materials in a matrix with a stiffness fourth-order tensor $\mathbb{C}_m$ ($K_m$, $\mu_m$) and volume fraction $\phi_m$. To conform to the theory of MRP homogenization, each phase can be distinguished by either the stiffness fourth-order tensor $\mathbb{C}_i$ ($K_i$, $\mu_i$), or by the particle size characterized by the radius $R_i$, or by both.

Thus, this model is denoted as the $(n+1)$ patterns MRPM, which includes $n$ three-phase patterns and one pattern of fictitious spherical inclusion of the pure matrix to account for the maximum packing effect. At the maximum volume fraction, we have $\phi=\sum_1^n c_i^M=\phi^M$, where $c_i^M$ denotes the volume fraction of phase $i$ ($i=1...n$) at the maximum volume fraction of the mixture. Using the same strategy as that of the 2 patterns MRPM model, we fix

$c_i = c_i^M$ for any value of $\phi_i$, and $\phi_i/c_i = \phi/\phi^M$, resulting in:

$$c_i = c_i^M, \qquad c_0 = 1 - \sum_i^n c_i^M = 1 - \phi^M \qquad \text{and} \qquad f_i = f = \frac{\phi_i}{c_i^M} = \frac{\phi}{\phi^M}. \tag{23}$$

The $(n+1)$ patterns MRPM for effective elastic properties of isotropic $(n+1)$ multiphase matrix-based composite material take the form:

$$(1-\phi^M)(K_m - K^e)A_0^s + \sum_{i=1}^{n} \left(\phi_i(K_i - K^e)A_i^{1s} + (c_i^M - \phi_i)(K_m - K^e)A_i^{2s}\right) = 0, \tag{24}$$

$$(1-\phi^M)(\mu_m - \mu^e)A_0^d + \sum_{i=1}^{n} \left(\phi_i(\mu_i - \mu^e)A_i^{1d} + (c_i^M - \phi_i)(\mu_m - \mu^e)A_i^{2d}\right) = 0. \tag{25}$$

It is worth noting that in equation (23), the volume fraction of phase $i$ at the maximum volume fraction of mixture, noted by $c_i^M$, is defined as a property of the mixture ($c_i^M = \frac{\phi^i}{\phi}\phi^M$). Thus, when a mixture is fixed, only one value of $c_i^M$ can be obtained.

## 4. Experimental validation

To evaluate the efficacy of the constructed MRPM approaches mentioned earlier, we investigate existing experimental and numerical data in the literature for the effective properties of different materials, such as non-Newtonian fluids reinforced by rigid particles, porous materials, and a Hookean solid material reinforced by solid elastic inclusions.

### *4.1. Monodisperse rigid particles in yield stress fluids*

In this subsection, we aim to validate the model's predictions against experimental data for suspensions of monodisperse rigid particles dispersed in yield stress fluids obtained by Mahaut et al. [11]. It is important to note that the materials and the elastic modulus measurement method used in [11] were specifically designed to study the purely mechanical contribution of an isotropic distribution of rigid monodisperse particles on the effective elastic modulus of suspensions. Figure 5 presents the empirical relationship between the effective shear modulus and the volume fraction of particles, where the volume fraction is close to the maximum packing value determined experimentally at 0.57 ($\phi^M = 0.57$). Further details on the experimental procedures and results can be found in [11, 12].

The predictions of the 2 patterns MRP approach, with geometric patterns estimated based on the mean distance between particles using equations (18), are shown in Figure 5. We observe significant differences between the theoretical calculations and the experimental data for high volume fractions of inclusions ($\phi > 0.3$), indicating that the MRP approach based on the mean distance between particles is not sufficient to accurately evaluate the

effective elastic properties at high volume fractions of inclusions. Furthermore, the MRP curve in Figure 5 is plotted with $\overline{\lambda}$ being the maximum value in (18), which provides the best curve for the approximation. When $\overline{\lambda}$ decreases, this curve deviates from the experimental data.

Fortunately, we find excellent agreement between the 2 patterns MRP approach, which is based on the maximum packing value from equations (20) (referred to as the MRPM), and the experimental data. Furthermore, the results are constructed entirely based on theoretical development and intrinsic material properties, without any fitting procedures. It is important to note that accurately predicting experimental effective values at high volume fractions for very high-contrast component property materials remains a significant challenge for theoretical micromechanical models. Therefore, the perfect coherence between the MRPM approach and the experimental data in Figure 5 is remarkable, demonstrating that the MRPM approach can account for some geometrical parameters and packing effects. This scheme is best suited for the monodisperse case and can be further explored for other applications, as presented in the following sections.

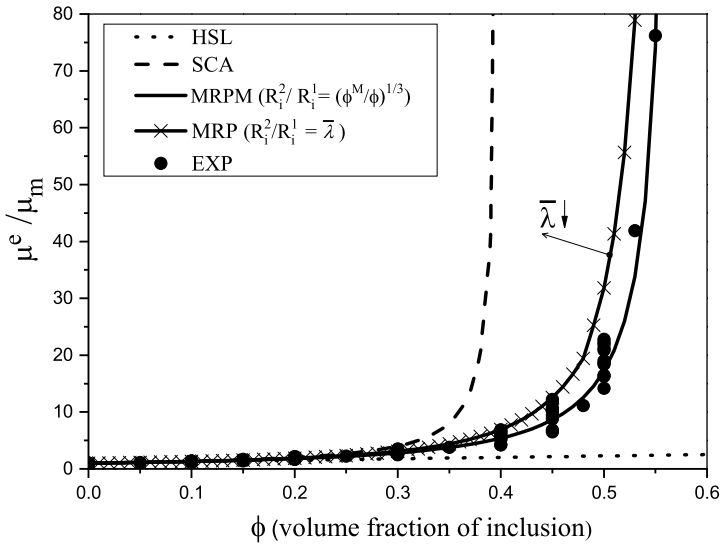


Figure 5: Dimensionless overall shear modulus of a dispersion of monodisperse rigid spheres dispersed in an elastic isotropic incompressible matrix as a function of the volume fraction. The solid curve represents the 2 patterns MRPM estimate for $\phi^M = 0.57$, the solid curve with a cross marker represents the MRP with $c_i$ defined from equation (18). The black circle dot indicates the experimental data, the dotted curve represents the Hashin-Shtrikman lower bound (HSL), and the dashed curve represents the classical self-consistent estimate (SCA).

### *4.2. Polydisperse rigid particles in yield stress fluids*

We now consider a more complex situation in which the composite contains randomly distributed rigid spheres of different sizes. Vu et al. [12] described an empirical procedure

and the results relating to the effective shear modulus for suspensions of monodisperse and bidisperse rigid particles distributed isotropically in incompressible yield stress fluids. Bidisperse mixtures of polystyrene beads with diameters of 80 $\mu$m and 315 $\mu$m (particle size ratio $\lambda = 3.94$) and bidisperse mixtures of glass beads with diameters of 40 $\mu$m and 330 $\mu$m ($\lambda = 8.25$) were studied. The particle mixture composition is defined by the ratio between the fine and total (fine and coarse) particle volume fraction denoted by $\xi$. The particles are dispersed in a volume of the suspending yield stress fluid, and the fluid-particle mixture is manually stirred in random directions to homogenize it and produce an isotropic material. The experimental overall shear modulus of six polydisperse mixtures characterized respectively by $\lambda = 3.94$, $\xi = 0.1$, 0.3 and $\lambda = 8.25$, $\xi = 0.1$, 0.2, 0.3, 0.5, plus one monodisperse mixture ($\lambda = 1$) for reference, is plotted in Figure 6.

To calculate $\phi^M$ for these mixtures, we applied the packing model of de Larrard [39], which provides a formula for the packing density of mixtures with sufficient accuracy for practical application. Generally, the packing model examines a polydisperse mixture of $n$ classes of spherical grains, in which each class is considered as an inclusion phase defined by the distribution function $P(\xi_i, R_i)$ with $\xi_i = \phi_i/\phi$ and $R_i$ the diameter of inclusion "i". Without loss of generality, the condition $R_i \geq R_{i+1}\ \forall i$ is considered. Thus, the maximum volume fraction of a given mixture is defined by

$$\Phi_i = \frac{\phi_i^M}{1 - \sum_{j=1}^{i-1}(1 - \phi_i^M + b_{ij}\phi_i^M(1 - 1/\phi_j^M))\xi_j - \sum_{j=i+1}^{n}(1 - a_{ij}\phi_i^M/\phi_j^M)\xi_j}, \tag{26}$$

$$\phi^M = \min_{1 \leq i \leq n}(\Phi_i). \tag{27}$$

Here, $\phi_i^M$ is the maximum volume fraction of the monodisperse suspension of phase "i", while $\Phi_i$ denotes the packing density of a composite mixture when the inclusion phases "i" are dominant. $a_{ij}$ (resp. $b_{ij}$) is a function that describes the loosening (resp. wall) effect. In this paper, we use the formula determined by Bournonville et al. [40] for a bidisperse mixture of particles:

$$a_{ij} = \left(1 - (1 - \frac{1}{\lambda_{ij}})^{1,13}\right)^{0,57} \quad , \quad \lambda_{ij} = \frac{R_i}{R_j} \quad \text{when} \quad i < j \tag{28}$$

$$b_{ij} = \left(1 - (1 - \frac{1}{\lambda_{ij}})^{1,79}\right)^{0,82} \quad , \quad \lambda_{ij} = \frac{R_j}{R_i} \quad \text{when} \quad i > j \tag{29}$$

Using equations (26-29) with $\phi_i^M = 0.57$, we compute the values of $\phi^M$ for six mixtures, which are presented in Figure 6.

According to the definition in section 3.2, the material studied in this section can be classified as a three-phase composite material, consisting of a phase matrix and two inclusion

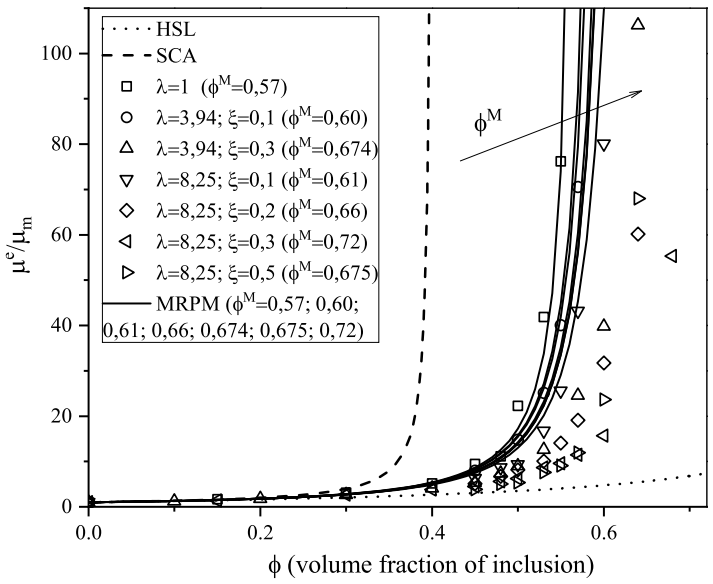


Figure 6: Dimensionless overall shear modulus of a dispersion of bidisperse rigid spheres in an elastic isotropic incompressible matrix as a function of the volume fraction of inclusion. The solid curve is the 2 patterns MRPM estimate for $\phi^M = (0,57; 0,6; 0,61; 0,66; 0,674; 0,675; 0,72)$. The markers are experimental data, the dotted curve is the Hashin-Shtrikman lower bound (HSL) and the dashed curve is the classical self-consistent estimate (SCA).

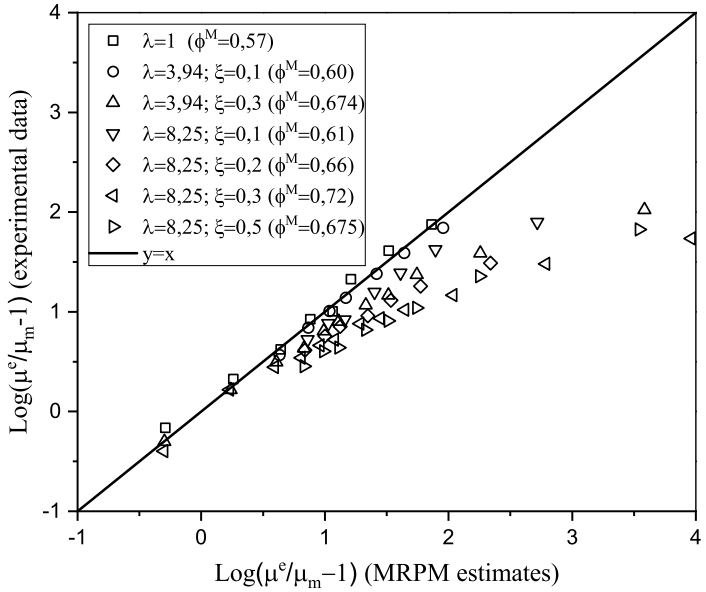


Figure 7: Dimensionless comparison between the experimental data and the MRPM in logarithmic coordinates. The solid line is the line $y = x$, the position where estimated value is equal to experimental value.

phases of different sizes. By incorporating the values of $\phi^M$ into the (2+1) patterns MRPM approach (equations (23, 24, 25)), we obtain the corresponding estimate curves, as shown in Figure 6. To elucidate the relationship between the experimental data and the MRPM approach, we plot a dimensionless comparison in logarithmic coordinates for all mixtures in Figure 7. We observe that the perfect agreement is reproduced for the monodisperse case, confirming the accuracy of the approach in this scenario. Moreover, as the particle volume fraction $\phi$ approaches zero, the model's prediction converges to the dilute solution $(1+2.5\phi)$, and the packing and polydispersity effects do not significantly affect the overall properties of such composites at low particle concentration. Conversely, when $\phi$ approaches $\phi^M$ ($\phi > 0.4$), the effective shear modulus obtained by the MRPM approach tends to infinity but does not accurately fit the experimental data for the mixture of $\phi^M > 0.6$. Vu et al. [12] have also demonstrated that the well-known Krieger-Dougherty equation $((1-\phi/\phi^M)^{-2.5\phi^M})$ does not agree with the experimental data, while the best fitting curve $((1-\phi/\phi^M)^{-2.5\times0.57})$ does not adhere to the dilute solution (known as the Einstein equation). Therefore, modeling such materials remains a challenge for both micromechanical and empirical approaches.

It is important to note that, according to the definition in equation (23), the volume ratio $f_i$ is equal for all matrix-inclusion patterns. This is equivalent to stating that the shape functions are identical for all matrix-inclusion patterns. Therefore, in the case where the elastic moduli of all inclusion phases are equal (i.e., solid rigid in this section), the (2+1) patterns MRPM approach (equations (24-25)) is identical to the 2 patterns MRPM approach (equations (21-22)). This could be an important factor contributing to the difference between the predictions and the experimental results shown in Figure 6.

To improve the effectiveness of our approach, several possibilities can be considered. Firstly, the form of equations (24-25) can be maintained while varying the volume fraction $f_i$ or volume $c_i$ of the matrix-inclusion patterns in equation (23). However, the correlation between these parameters and the microstructure of the composites has been debated. Alternatively, a two-step MRPM approach associated with the packing model can be planned. In the first step, the overall moduli of elasticity can be calculated using the 2 patterns MRPM model (equations (21-22)) for a two-phase material consisting of a matrix and a dominant phase inclusion of size 1. The maximum packing of phase 1 $\phi_1^M$ can then be calculated using the packing model, which accounts for the wall/loosening effect caused by the interaction between phases 1 and 2. In the second step, the process can be repeated using the matrix that is the effective medium calculated from the first step and phase 2. A multi-step MRPM model can be extended to multiphase materials by multiplying the steps accordingly. Note that this sequential model would be appropriate when there is a significant size difference between types of particles. When the sizes are close to each other, the value of maximum packing in each step will play a regulatory role. To ensure that these proposed approaches appear as pure analytical approaches that reflect physical reality, strong correlations between

the geometric parameters of the MRPM model ($f_i$, $c_i$...) and the associated packing model must be established. With the current data, there is not enough information to present agreeable results or draw reasonable conclusions. Nonetheless, in Section 5, a detailed proposal for a more flexible and effective solution will be provided.

### *4.3. Porous materials*

In this subsection, we aim to validate the effectiveness of the MRPM approach for modeling porous media. Figure 8 shows a comparison between the MRPM approach and experimental data for the dimensionless elastic modulus of lightweight concrete, as measured by Le Roy et al. [41] and Miled et al. [42]. In this comparison, the Poisson ratio ($\nu_m$) of the solid matrix is assumed to be equal to 0.2 [43]. For $\phi^M = 0.57$, there is a strong agreement between the experimental data and the MRPM approach for porosity values up to 0.4. Differences between the MRPM estimate at $\phi^M = 0.57$ and the experimental data for higher porosity values may be due to changes in porous space under loading. Notably, the best fit for the maximum porosity is equal to 0.73, which is very close to the collapsed value of porosity (0.74) reported in [41].

In the second example, Figure 9 presents a similar comparison for a ceramic material, comparing experimental data from [44] with the numerical simulation work of Roberts et al. [45], the upper Hashin-Shtrikman bound, and the MRPM approach. The elastic modulus ($E_m$) and shear modulus ($\mu_m$) of the matrix are 386.1 GPa and 162.7 GPa, respectively. The predictions of the MRPM approach at $\phi^M = 0.57$ show good agreement with both numerical and experimental data for porosity values up to 0.4. Furthermore, if we accept an adaptive strategy that considers $\phi^M$ as a free parameter that can be obtained by fitting it with experimental data, the best fit for the maximum value of porosity is 0.62, which is close to the maximum packing of random sphere close packing (0.64).

### *4.4. Hookean solid composite materials*

To further assess the proposed approach's ability to predict the effective elastic properties of two-phase reinforced composites, this subsection presents a comparison between the theoretical predictions and the experimental data obtained by Smith [46]. Smith investigated the mechanical contribution of reinforced monodisperse glass spheres embedded in a solid epoxy polymer matrix. The tested material has the following mechanical properties: the elastic modulus and Poisson's ratio of glass are $E_i = 76$ GPa and $\nu_i = 0.23$, respectively, while $E_m = 3.01$ GPa and $\nu_m = 0.349$ for the matrix phase.

Figures 10 and 11 show the comparison between the experimental data of Smith [46], the upper and lower Hashin-Shtrikman bounds, and our MRPM model's predictions for the elastic modulus and shear modulus, computed using $\phi^M = 0.56$, which is close to the value of 0.57 found experimentally by Mahaut et al. [11] for similar material. Furthermore, to demonstrate

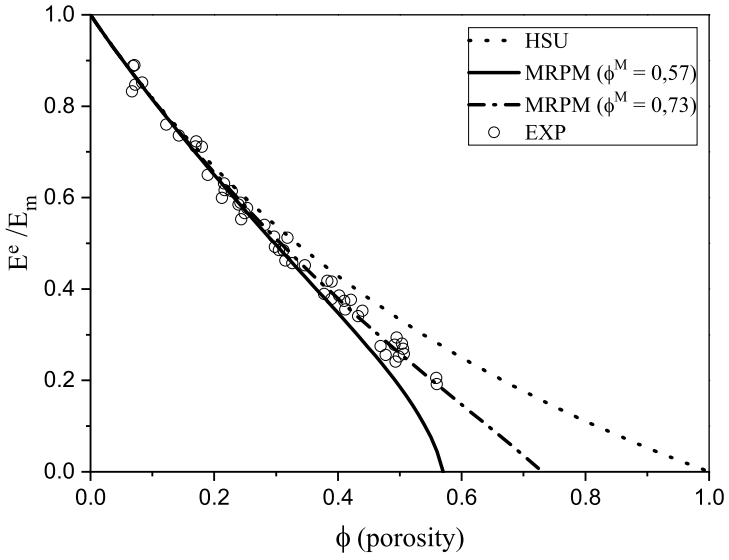


Figure 8: Dimensionless elastic modulus of lightweight concrete with a Poisson ratio $\nu_m = 0.2$ as a function of porosity. The solid and dash-dot curves represent the 2 patterns MRPM estimates for $\phi^M = 0.57$ and 0.73, respectively. Open circles indicate experimental data, and the dotted curve is the Hashin-Shtrikman upper bound (HSU).

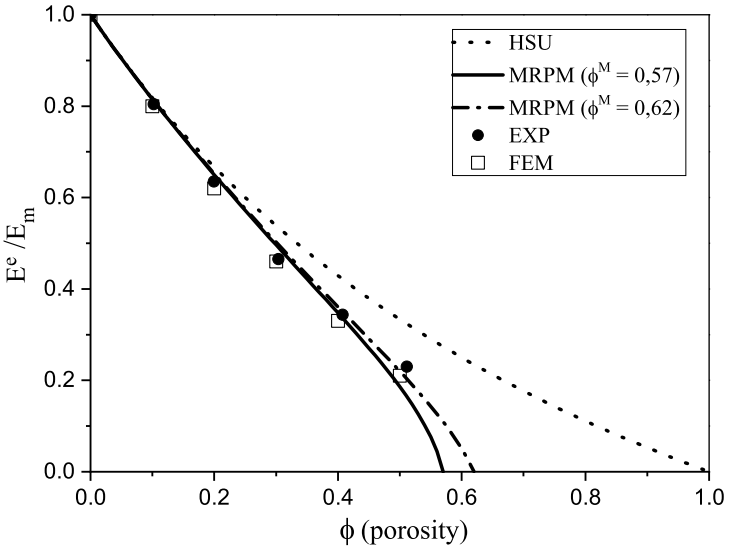


Figure 9: Dimensionless elastic modulus of ceramic with matrix elastic modulus $E_m = 386.1$ GPa and matrix shear modulus $\mu_m = 162.7$ GPa as a function of porosity. The solid and dash-dot curves represent the 2 patterns MRPM estimates for $\phi^M = 0.57$ and 0.62, respectively. The black dots indicate experimental data, the white squares are numerical data, and the dotted curve is the Hashin-Shtrikman upper bound (HSU).

the effectiveness of the MRPM method, both the classical self-consistent approach (SCA) and the generalized self-consistent approach (GSCA) proposed by Christensen and Lo [19] are also depicted in the figures. The SCA corresponds to the MRPM model with $\phi^M = \phi_i$, while the

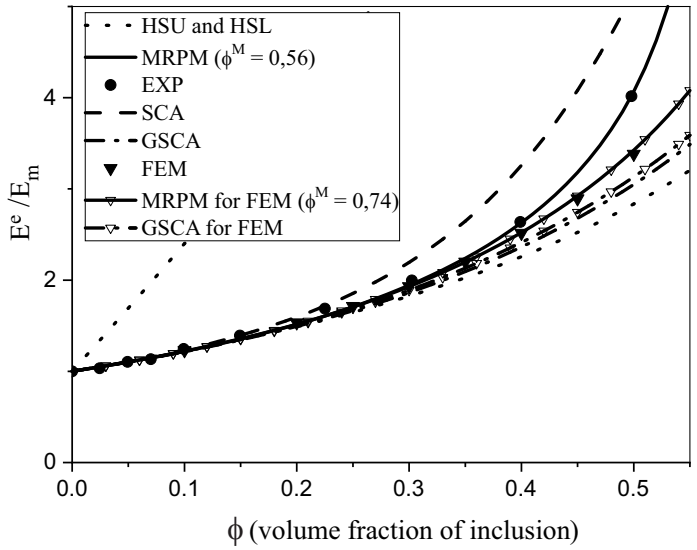


Figure 10: Dimensionless overall elastic modulus of a dispersion of monodisperse glass spheres in an elastic isotropic epoxy polymer matrix as a function of the volume fraction of solid. For experimental data: the solid curve is the MRPM estimate for $\phi^M = 0.56$, the black circle represents experimental data, the dashed curve is the classical self-consistent estimate (SCA), the dash-dotted curve is the generalized self-consistent approximation (GSCA), and the dotted curves are the Hashin-Shtrikman upper and lower bounds (HSU and HSL). For finite element modeling (FEM): the solid curve with triangle symbol is the MRPM estimate for $\phi^M = 0.74$, the black triangle represents numerical data, and the dash-dotted curve with triangle symbol is the generalized self-consistent approximation (GSCA).

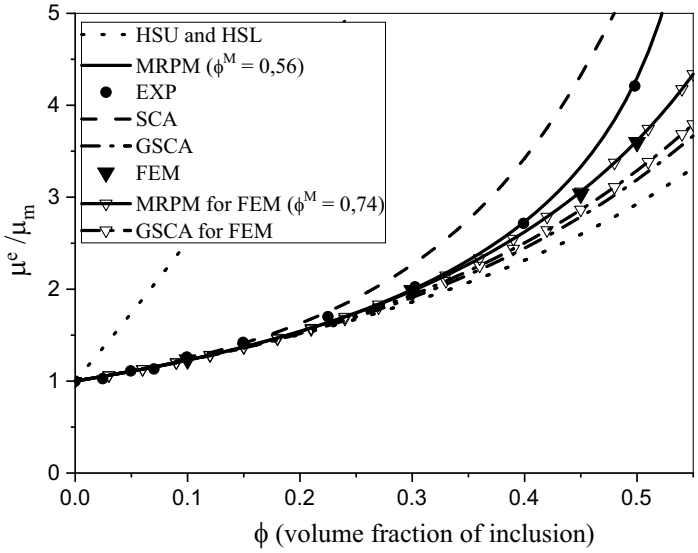


Figure 11: Dimensionless overall shear modulus of a dispersion of monodisperse glass spheres in an elastic isotropic epoxy polymer matrix as a function of the volume fraction of solid. For experimental data: the solid curve is the MRPM estimate for $\phi^M = 0.56$, the black circle represents experimental data, the dashed curve is the classical self-consistent estimate (SCA), the dash-dotted curve is the generalized self-consistent approximation (GSCA), and the dotted curves are the Hashin-Shtrikman upper and lower bounds (HSU and HSL). For finite element modeling (FEM): the solid curve with triangle symbol is the MRPM estimate for $\phi^M = 0.74$, the black triangle represents numerical data, and the dash-dotted curve with triangle symbol is the generalized self-consistent approximation (GSCA).

GSCA corresponds to the MRPM model with $\phi^M = 1$. These figures reveal good agreement between the MRPM model's predictions and the experimental data at any volume fraction of inclusion, thus confirming the accuracy and merit of the MRPM model.

Despite the GSCA being an optimal analytical model for predicting the numerical effective elastic moduli of microstructures, as reported in several publications [47, 48, 49, 50], we observe a significant discrepancy between its predictions and experimental data (up to 24% at $\phi = 0.5$). To clarify this issue further, we present numerical results of Segurado et al. [47] for a similar composite material, consisting of an epoxy matrix ($E_m = 3$ GPa, $\nu_m = 0.38$) reinforced with glass spheres ($E_i = 70$ GPa, $\nu_i = 0.2$), in Figures 10 and 11, along with the GSCA and MRPM models using the corresponding material parameters for finite element simulations. The value of $\phi^M$ considered in our analysis is 0.74, which is reported in section 3.5 of [51] when the algorithm used for generation allows for a random microstructure volume fraction of 74%, approaching the theoretical maximum dense packing arrangement for spheres of identical size. The correlation of the GSCA with numerical simulations is consistent with previous studies, while the MRPM model's perfect agreement demonstrates its effectiveness for various experimental and numerical data.

## 5. The refined MRPM

The MRPM, which is distinct from other classical effective medium approximations referenced in Section 2, includes a maximum volume fraction parameter that can be defined both theoretically and experimentally. In Section 4, we demonstrate the positive effectiveness and ability of the MRPM through good agreement between theoretical predictions and experimental data obtained for several composite materials, including monodisperse rigid particles in yield stress fluid material, Hookean solid composite materials reinforced by monodisperse inclusions, and some types of porous materials. However, for suspensions of polydisperse rigid particles in yield stress fluids, the MRPM approach-experimental data correlations are weak at volume fractions close to maximum packing values. Despite $\phi^M$ serving as a fitting parameter, the agreement between the MRPM estimates and the empirical data for the effective shear modulus of such suspensions is unsatisfactory. This may be due to the fact that in polydisperse cases, the shape of the matrix becomes more tortuous, requiring adjustments to the formula of the model to adapt to the configuration.

The literature on inclusion-matrix composite materials [52, 53, 54] demonstrates a monotonic relationship between the effective elastic properties of these composites and the shape of the inclusions. This finding motivates a simple modification of the MRPM approach that permits the model to better predict polydisperse systems while still maintaining its ease of use. Specifically, we propose using a spheroidal shape for the first pattern, with a rapport ratio $r = b/a$ representing the semi-axes along the principal directions. This modified approach,

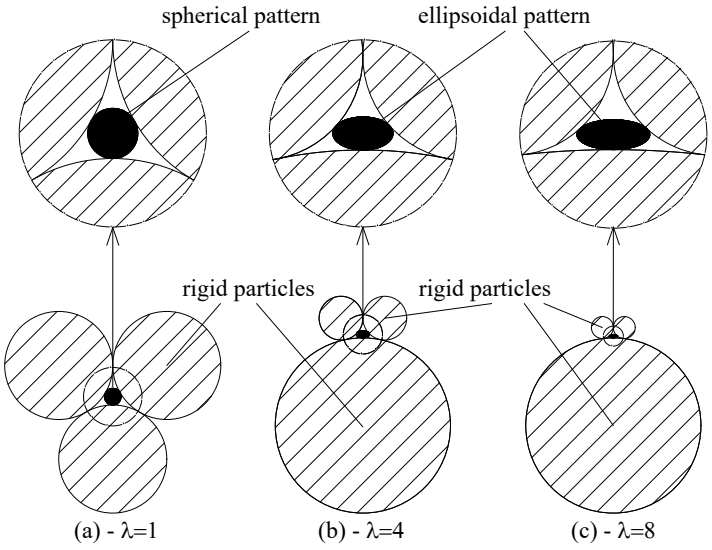


Figure 12: Illustrations of the shape of the first pattern at $\phi = \phi^M$.

called RMRPM, accounts for the shape parameter $r$. In Figure 12, we illustrate the effect of polydispersity on the first pattern's shape for three particle size ratios ($\lambda = 1, 4, 8$), where $\lambda = 1$ denotes a spherical shape and $\lambda = 4, 8$ denote ellipsoidal shapes (with $r$ decreasing as $\lambda$ increases) for the first pattern. It is necessary to discuss that the question of the physical meaning of the parameter $r$ is intriguing but challenging to demonstrate quantitatively. As depicted in Figure 12 (a), for a monodisperse mixture, it is evident that the space between particles at maximum packing is centrally symmetric. Thus, we can assume a spherical shape (with a centrally symmetric shape as well) to represent the matrix of material within that space, which yields excellent results (as seen in Figure 5). However, in the case of a polydisperse mixture, the space between particles becomes more complex and is no longer centrally symmetric as shown in Figure 12 (b, c). Therefore, there is no reason to constrain the shape of the fictitious pattern to be a sphere in this case. In fact, it has been demonstrated that assuming a spherical shape leads to poor results, as depicted in Figure 6. These are the primary qualitative justifications for establishing the RMRPM model in the section.

Next, to conform with the RMRPM approach, we express the dilute solution of the first pattern "0" as follows:

$$\mathbb{C}_0 = \mathbb{C}^e + c_0(\mathbb{C}_m - \mathbb{C}^e) : (\mathbb{I} + (\mathbb{C}_m - \mathbb{C}^e) : (\mathbb{C}^e)^{-1} : \mathbb{S}_E) \tag{30}$$

where the term

$$\mathbb{A}_0 = (\mathbb{I} + (\mathbb{C}_m - \mathbb{C}^e) : (\mathbb{C}^e)^{-1} : \mathbb{S}_E) \tag{31}$$

represents the strain localization fourth order tensor of an isotropic spheroidal inclusion ($\mathbb{C}_m$)

embedded in an effective infinite domain ($\mathbb{C}^e$). The Eshelby tensor $\mathbb{S}_E$ is generally given in terms of elliptic integrals of the first and second kind. In the case of a three-dimensional spheroidal inclusion in a local orthonormal frame ($\underline{x}_j$, $j = 1..3$), with semi axes $a_1 = a_2 = a$ and $a_3 = b$ whose local symmetry axis is aligned in the $x_3$ direction, the elliptic integrals can be evaluated analytically (see page 449 of [3]). The dilute suspension result of the pattern "0" for randomly oriented spheroids (hence the effective medium is isotropic) can be obtained from the isotropic averages of the tensor $\mathbb{A}_0$:

$$\overline{\mathbb{C}}_0 = \mathbb{C}^e + c_0(\mathbb{C}_m - \mathbb{C}^e) : \overline{\mathbb{A}}_0 \tag{32}$$

where

$$\overline{\mathbb{A}}_0 = 3\overline{A}_0^s\mathbb{J} + 2\overline{A}_0^d\mathbb{K}, \qquad \mathbb{C}(\alpha) = 3K(\alpha)\mathbb{J} + 2\mu(\alpha)\mathbb{K}, (\alpha) = \{_i, _m, ^e\}, \tag{33}$$

$$\mathbb{J} = 1/3\mathbf{1} \otimes \mathbf{1} \qquad , \qquad \mathbb{K} = \mathbb{I} - \mathbb{J}, \tag{34}$$

and

$$\overline{A}_0^s = \frac{A_{0iijj}}{3} \qquad , \qquad \overline{A}_0^d = \frac{1}{5}(A_{0ijij} - \frac{A_{0iijj}}{3}). \tag{35}$$

Here, $\mathbb{I}$ and $\mathbf{1}$ denote the fourth and second-order (symmetric) identity tensors, respectively. In equation (35), $i$ and $j$ are repeated indices from 1 to 3 using the Einstein summation convention. The symbols $\overline{A}_0^s$ and $\overline{A}_0^d$ respectively denote the isotropic averages of the spherical and deviatoric components of the strain localization tensor, as discussed in eqs. (1, 2). These quantities can be computed directly from eqs. (31-35) and their explicit expressions, derived in [55], are presented in Appendix B for use in engineering applications.

As discussed in section 4.2, the simple geometric approximation leads to equations (24-25) and equations (21-22) being equivalent. Therefore, by applying eqs. (30-35) in (21-22), we obtain the refined MRPM approach for the polydisperse inclusion-matrix composite (the RMRPM approach):

$$(1 - \phi^M)(K_m - K^e)\overline{A}_0^s + \phi_i(K_i - K^e)A_i^{1s} + (\phi^M - \phi_i)(K_m - K^e)A_i^{2s} = 0, \tag{36}$$

$$(1 - \phi^M)(\mu_m - \mu^e)\overline{A}_0^d + \phi_i(\mu_i - \mu^e)A_i^{1d} + (\phi^M - \phi_i)(\mu_m - \mu^e)A_i^{2d} = 0. \tag{37}$$

Six scalar quantities $A_i^{1s}$, $A_i^{2s}$, $A_i^{1d}$, $A_i^{2d}$, $\overline{A}_0^s$, and $\overline{A}_0^d$, are presented in Appendix A and B. The parameter $r$ in $\overline{A}_0^s$ and $\overline{A}_0^d$ is a free parameter of the model, and it can take any value from 0 to infinity.

To assess the effectiveness of the RMRPM approach, we first investigate the influence of $r$ on the effective shear modulus of the material shown in Figure 2. We consider $\phi^M = 0.64$ and $\phi = 0.5$ at $r = 0 \to \infty$, where fictitious inclusion shapes change from a disk at $r = 0$

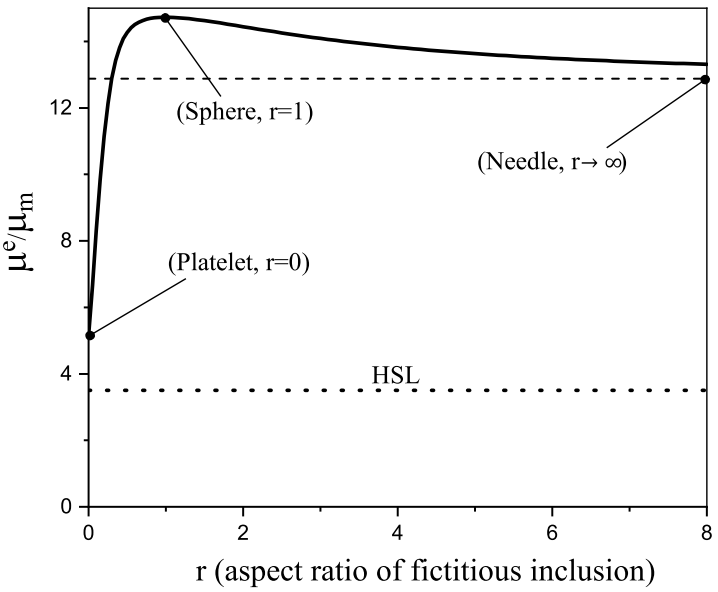


Figure 13: Dimensionless effective elastic shear modulus of a dispersion of rigid spheres in an elastic isotropic incompressible matrix as a function of the aspect ratio of the fictitious inclusion. The solid curve is the RMRPM self-consistent computed for $\phi = 0.5, \phi^M = 0,64$. The dotted curve is the Hashin-Shtrikman lower bound (HSL) and the dashed line is the convergent value at $r \to \infty$.

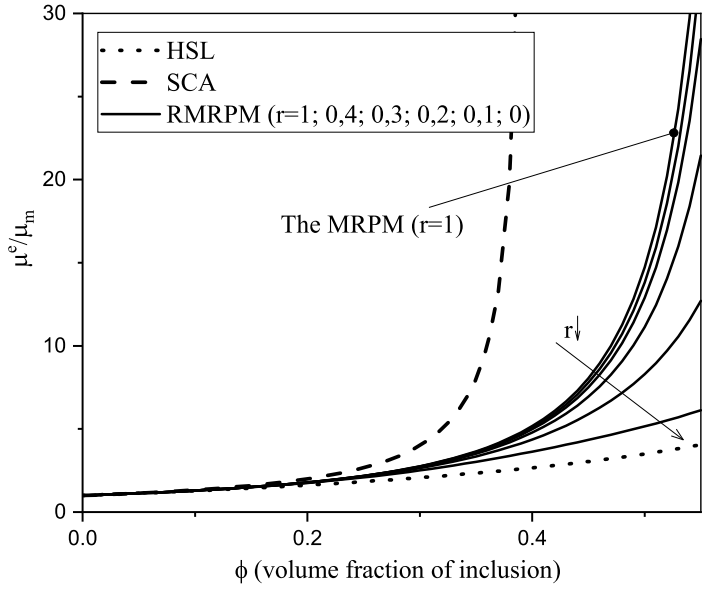


Figure 14: Dimensionless overall shear modulus of a dispersion of monodisperse rigid spheres in an elastic isotropic incompressible matrix as a function of the volume fraction of solid. The solid curves are the RMRPM approach's estimates for $\phi^M = 0,64$ and $r = (1; 0,4; 0,3; 0,2; 0,1; 0)$. The dotted curve is the Hashin-Shtrikman lower bound (HSL) and the dashed curve is the classical self-consistent estimate (SCA).

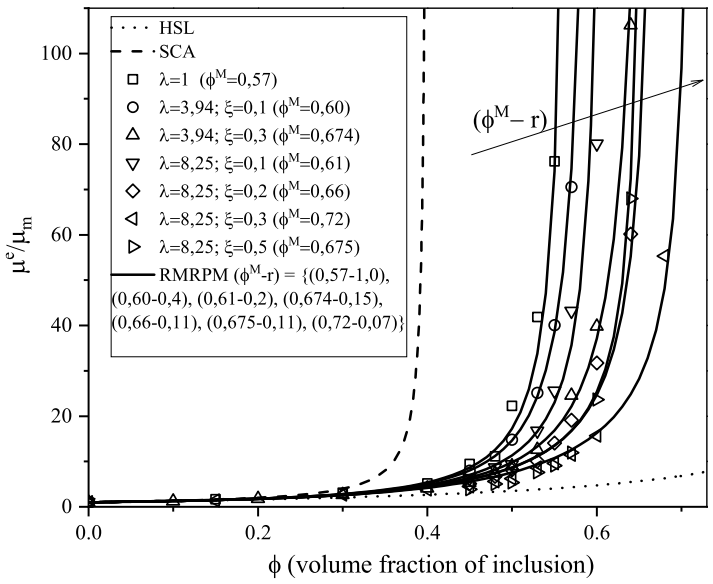


Figure 15: Dimensionless overall shear modulus of a dispersion of bidisperse rigid spheres in an elastic isotropic incompressible matrix as a function of the volume fraction of solid. The solid curves are the RMRPM approach's estimates for $(\phi^M - r) = \{(0,57-1);\ (0,6-0,4);\ (0,61-0,2);\ (0,74-0,15);\ (0,66-0,11);\ (0,675-0,11);\ (0,72-0,07)\}$. The markers are experimental data, the dotted curve is the Hashin-Shtrikman lower bound (HSL) and the dashed curve is the classical self-consistent estimate (SCA).

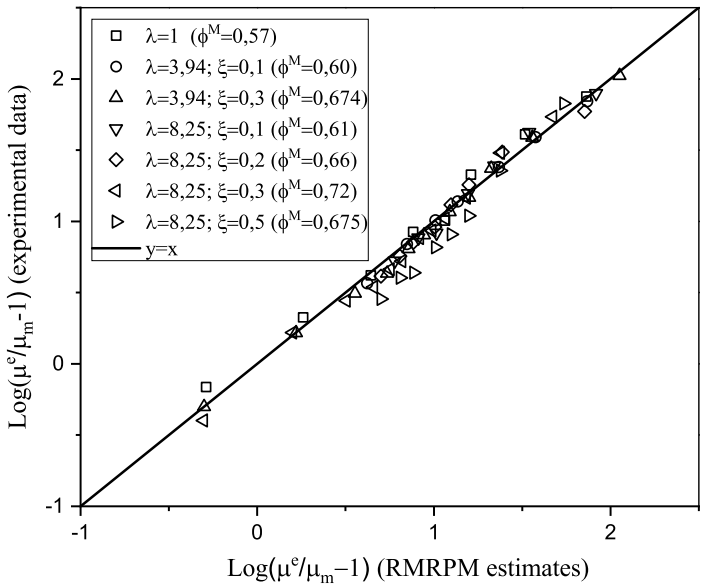


Figure 16: Dimensionless comparison between the experimental data and the RMRPM approach's estimate in logarithmic coordinates.

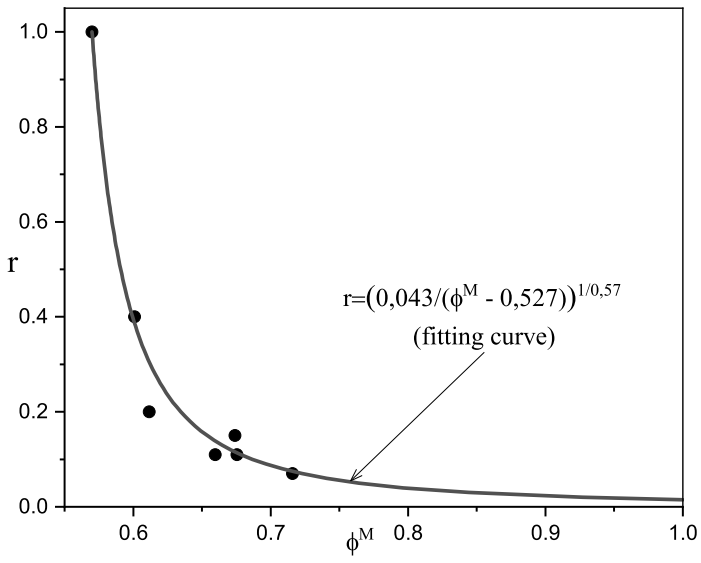


Figure 17: $\phi^M - r$ relationship.

(corresponding to the minimum value of effective shear modulus) through a sphere at $r = 1$ (maximum value) to a needle at $r \to \infty$ (convergent value) (see Figure 13). Similar curves can be obtained for different values of $\phi$ and $\phi^M$, while inverse behavior curves (with a maximum value at $r = 0$ and minimum value at $r = 1$) can be found for materials with inclusion stiffness softer than the matrix, such as porous materials. These results allow us to restrict the variation of $r$ from 0 to 1, corresponding to the oblate shape of the fictitious inclusion, for further applications.

To better understand the effects of $r$ on the approach's estimates, we present some calculations in Figure 14. We fix $\phi^M$ at 0.64 and plot the RMRPM approach's curves for different values of $r$ (1, 0.4, 0.3, 0.2, 0.1, 0). The RMRPM tends to the MRPM at $r = 1$, and the RMRPM approaches the dilute solution when the volume fraction is small for any value of $r$. Differences arise in situations where the volume fraction is greater. In Figure 14, we observe that the RMRPM tends to the HSL bound when $r$ tends to 0, and the RMRPM covers a wide range of effective elastic modulus values, depending on $r$, at volume fractions close to the maximum packing, demonstrating the flexibility and effectiveness of the proposed approach.

Applying the proposed model for the polydisperse situation in Section 4.2, we find that the RMRPM approach yields better prediction curves with $r < 1$. Figures 15 and 16 show the comparative calculations for the different mixtures discussed above, where seven types of material corresponding to seven values of $\phi^M$ (0.57, 0.60, 0.61, 0.65, 0.674, 0.675, 0.71) are fitted by the least squares method, corresponding to seven values of $r$ respectively (1, 0.4, 0.2, 0.11, 0.15, 0.11, 0.07). We observe a strong agreement between the experimental

data and the RMRPM constructed based on the micromechanical framework that respects HS bounds and the Einstein equation when $\phi$ tends to zero for all mixtures. Furthermore, the relationship between $r$ and $\phi^M$ shows a strong correlation that can be simulated by a fitting curve (Figure 17),

$$r = \left( \frac{1 - \phi^M_{r=1}}{10\phi^M - (11\phi^M_{r=1} - 1)} \right)^{1/\phi^M_{r=1}} \qquad \text{with} \qquad \phi^M_{r=1} = 0,57. \tag{38}$$

In this regard, the RMRPM appears to be more of an analytical approach than a fitting procedure based on an analytical homogenization strategy itself, which is remarkable.

## 6. Conclusions

In this study, we presented a new micromechanical approach to predict the effective elastic properties of composites with high particle concentrations and high-contrast component properties. We established coupled self-consistent equations for several configurations based on the Morphological Representative Pattern scheme, which accounts for packing and size effects through a simple geometric approximation of a fictitious matrix pattern's size and shape. Our research yielded the following conclusions:

Firstly, the 2 patterns Morphological Representative Pattern approach with the packing effect (MRPM) agreed perfectly with experimental data for suspensions of monodisperse solid particles in various matrices with a maximum packing fraction value of 0.57, as determined experimentally. These agreements also applied to some porous materials, where the maximum packing fraction could be determined experimentally or play a role as a fitting parameter in the adaptive strategy sense. In addition, a comparison has been made between experimental results and numerical results obtained using the finite element method, as well as predictions from the MRPM model (Figures 10 and 11). The results obtained for the epoxy/glass material demonstrate that the MRPM model is quite flexible and effective for both experimental and numerical data, compared to the GSCA model, which has been reported as an optimal model in some recent studies. However, for monodisperse solid particles dispersed in an incompressible matrix, the GSCA model is found to be more coherent with numerical data [50]. Therefore, it is crucial to carefully consider the discrepancy between numerical and experimental results, as well as the assessment of the method's effectiveness proposed in the current study, in future research.

Secondly, by combining the self-consistent equations (eqs. (36, 37)), the packing model (eqs. (26-29)), and the correlation curve $r - \phi^M$ (38), we proposed an analytical model to compute the effective shear modulus of a suspension of bidisperse particles in a yield stress fluid up to the maximal packing points of the interactions (RMRPM). This model exhibited good coherence with the experimental data and respected the micromechanical bounds. It

was explicit, flexible, and readily applicable in broad engineering contexts. In cases where there was insufficient data to determine the maximum packing fraction precisely or where the best simulation curve was desired, the RMRPM approach may be considered as a fitting procedure based on the analytical homogenization approach with one or two free parameters ($\phi^M$ and $r$).

Thirdly, Chateau et al. [56] proposed an analytical formula for isotropic suspensions of non-colloidal particles in yield stress fluids that links the overall yield stress, overall elastic moduli, and solid volume fraction ($\tau^e/\tau_m = \sqrt{(1-\phi)\mu^e/\mu_m}$). By combining this formula with our results, we propose a novel micromechanical model for both the elastic modulus and the yield stress. The wide application potential of this material type highlights the significance of this method.

We plan to further develop this approach to predict the elastic moduli and damage properties of very high concentrations materials, such as syntactic foam composites, where spherical reinforced void particles are dispersed in matrix material up to 75% volume fraction [30, 57]. Furthermore, future work will focus on validating the models for both numerical and experimental data for cases of anisotropic particle distribution and/or polydisperse multicomponent matrix-inclusion composite materials.

**Acknowledgments**

This research is funded by Ministry of Education and Training under grand number B2023-XDA-03 and B2022-GHA-06.

## Appendix A. Expressions of $A_i^{1s}, A_i^{2s}, A_i^{1d}, A_i^{2d}$

$$\begin{cases} A_i^{1s} = \frac{(3\,K^e+4\,\mu^e)(3\,K_m+4\,\mu_m)}{(3\,K_m+4\,\mu^e)(3\,K_i+4\,\mu_m)+12\,y^3(\mu^e-\mu_m)(K_m-K_i)} \\ A_i^{2s} = \frac{(3\,K^e+4\,\mu^e)(3\,K_i+4\,\mu_m)}{(3\,K_m+4\,\mu^e)(3\,K_i+4\,\mu_m)+12\,y^3(\mu^e-\mu_m)(K_m-K_i)} \end{cases} \tag{A.1}$$

$$\begin{cases} A_i^{1d} = 225\,\frac{(1-\nu^e)(1-\nu_m)X_0\left(-4\,(X_0-1)\left(\eta_1\,y^7-\eta_2\,(7-10\,\nu_m)\right)+35\,\eta_2\,(1-\nu_m)\right)}{\Delta} \\ A_i^{2d} = 15\,\frac{(1-\nu^e)X_0\left((X_0-1)\left(A+60\,y^3(1-\nu_m)\left(\eta_1\,y^7-\eta_2\,(7-10\,\nu_m)\right)\right)+35\,(1-\nu_m)\eta_2\,\eta_3\left(1-y^3\right)\right)}{(1-y^3)\Delta} \end{cases} \tag{A.2}$$

$$
\begin{cases}
y = R_i^1/R_i^2 = f_i^{1/3} \\
A = -4\,(\eta_3 - 2\,\alpha\,(4 - 5\,\nu_m)\,y^3)\,(\eta_1\,y^7 - \eta_2\,(7 - 10\,\nu_m)) - 126\,\alpha\,\eta_2\,y^3\,(1 - y^2)^2 \\
C = -\,(\eta_3 + \alpha\,(7 - 5\,\nu_m)\,y^3)\,(4\,\eta_1\,y^7 + \eta_2\,(7 + 5\,\nu_m)) - 126\,\alpha\,\eta_2\,y^3\,(1 - y^2)^2 \\
X_0 = \mu^e/\mu_m \\
\eta_1 = (49 - 50\,\nu_m\nu_i)\,\alpha + 35\,(1 + \alpha)\,(\nu_i - 2\,\nu_m) + 70\,\nu_i - 35\,\nu_m \\
\eta_2 = (7 + 5\,\nu_i)\,(1 + \alpha) + 28 - 40\,\nu_i \\
\eta_3 = 2\,(1 + \alpha)\,(4 - 5\,\nu_m) + 7 - 5\,\nu_m \\
\alpha = \mu_i/\mu_m - 1 \\
\Delta = (2\,(4 - 5\,\nu^e)\,C + (7 - 5\,\nu^e)\,AX_0)\,(X_0 - 1) + ... \\
\qquad ...525\,\eta_2\,(1 - \nu_m)\,(2\,\alpha\,(\nu_m - \nu^e)\,y^3 + (1 - \nu^e)\,\eta 3)\,X_0 \\
\nu_i = (3K_i - 2\mu_i)/(6K_i + 2\mu_i), \qquad \nu_m = (3K_m - 2\mu_m)/(6K_m + 2\mu_m) \\
\nu^e = (3K^e - 2\mu^e)/(6K^e + 2\mu^e)
\end{cases}
\tag{A.3}
$$

## Appendix B. Expressions of $\overline{A}_0^s, \overline{A}_0^d$

$$
\begin{cases}
\overline{A}_0^s = F1/F2 \\
\overline{A}_0^d = 1/5\left(2\,F3^{-1} + F4^{-1} + (F4F5 + F6F7 - F8F9)(F2F4)^{-1}\right) \\
F1 = 1 + AA\,(3/2\,f + 3/2\,\theta - R\,(3/2\,f + 5/2\,\theta - 4/3)) \\
F2 = 1 + AA\,(1 + 3/2\,f + 3/2\,\theta - 1/2\,R\,(3\,f + 5\,\theta)) + ... \\
\qquad ... + B\,(3 - 4\,R) + 1/2\,AA\,(AA + 3\,B)\,(3 - 4\,R)\,(f + \theta - R\,(2\,\theta^2 + f - \theta)) \\
F3 = 1 + AA\,(1 - f - 3/2\,\theta + R\,(f + \theta)) \\
F4 = 1 + 1/4\,AA\,(f + 3\,\theta - R\,(f - \theta)) \\
F5 = AA\,(R\,(f + \theta - 4/3) - f) + B\theta\,(3 - 4\,R) \\
F6 = 1 + AA\,(1 + f - R\,(f + \theta)) + B\,(1 - \theta)\,(3 - 4\,R) \\
F7 = 2 + 1/4\,AA\,(3\,f + 9\,\theta - R\,(3\,f + 5\,\theta)) + B\theta\,(3 - 4\,R) \\
F8 = AA\,(1 - 2\,R + 1/2\,f\,(R - 1) + 1/2\,\theta\,(5\,R - 3)) + B\,(1 - \theta)\,(3 - 4\,R) \\
F9 = AA\,(f\,(R - 1) - R\theta) + B\theta\,(3 - 4\,R) \\
AA = \mu_m/\mu^e - 1 \\
R = (1 - 2\nu^e)/(2 - 2\nu^e) \\
f = r^2(2 - 3\theta)(r^2 - 1)^{-1} \\
B = 1/3\,(K_m/K^e - \mu_m/\mu^e)
\end{cases}
\tag{B.1}
$$

$$
\theta = \begin{cases}
r\left(\arccos(r) - r\sqrt{-r^2 + 1}\right)(-r^2 + 1)^{-3/2} & : \quad 0 \le r \le 1 \quad \text{(oblate)} \\
r\left(r\sqrt{r^2 - 1} - \operatorname{arccosh}(r)\right)(r^2 - 1)^{-3/2} & : \quad 1 \le r \qquad \text{(prolate)}
\end{cases}
\tag{B.2}
$$

## References


[1] R. Christensen, Mechanics of composite materials, John Wiley & Sons. Inc., 1979.

[2] S. Nemat-Nasser, M. Hori, Micromechanics: overall properties of heterogeneous solids, Elsevier, Amsterdam, 1999.

[3] S. Torquato, Random Heterogeneous Materials. Interdisciplinary Applied Mathematics, Vol. 10, Springer-Verlag, New York, 2002.

[4] L. Dormieux, D. Kondo, F.-J. Ulm, Microporomechanics, John Wiley & Sons, 2006.

[5] J. Willis, Bounds and self-consistent estimates for the overall properties of anisotropic composites, Journal of the Mechanics and Physics of Solids 25 (3) (1977) 185–202.

[6] B. Budiansky, On the elastic moduli of some heterogeneous materials, Journal of the Mechanics and Physics of Solids 13 (4) (1965) 223–227.

[7] V. D. Bruggeman, Berechnung verschiedener physikalischer konstanten von heterogenen substanzen. i. dielektrizitätskonstanten und leitfähigkeiten der mischkörper aus isotropen substanzen, Annalen der physik 416 (7) (1935) 636–664.

[8] A. Norris, A differential scheme for the effective moduli of composites, Mechanics of materials 4 (1) (1985) 1–16.

[9] T. Mori, K. Tanaka, Average stress in matrix and average elastic energy of materials with misfitting inclusions, Acta metallurgica 21 (5) (1973) 571–574.

[10] J. D. Eshelby, The determination of the elastic field of an ellipsoidal inclusion, and related problems, in: Proceedings of the Royal Society of London A: Mathematical, Physical and Engineering Sciences, Vol. 241, The Royal Society, 1957, pp. 376–396.

[11] F. Mahaut, X. Chateau, P. Coussot, G. Ovarlez, Yield stress and elastic modulus of suspensions of noncolloidal particles in yield stress fluids, Journal of Rheology (1978-present) 52 (1) (2008) 287–313.

[12] T.-S. Vu, G. Ovarlez, X. Chateau, Macroscopic behavior of bidisperse suspensions of noncolloidal particles in yield stress fluids, Journal of Rheology (1978-present) 54 (4) (2010) 815–833.

[13] A. Norris, A. Callegari, P. Sheng, A generalized differential effective medium theory, Journal of the Mechanics and Physics of Solids 33 (6) (1985) 525–543.

[14] N. Phan-Thien, D. Pham, Differential multiphase models for polydispersed suspensions and particulate solids, Journal of Non-Newtonian Fluid Mechanics 72 (2) (1997) 305–318.

[15] N. Phan-Thien, D. Pham, Differential multiphase models for polydispersed spheroidal inclusions: thermal conductivity and effective viscosity, International Journal of Engineering Science 38 (1) (2000) 73–88.

[16] M. Markov, V. Levine, A. Mousatov, E. Kazatchenko, Elastic properties of double-porosity rocks using the differential effective medium model, Geophysical Prospecting 53 (5) (2005) 733–754.

[17] M. Markov, V. Levin, A. Mousatov, E. Kazatchenko, Generalized dem model for the effective conductivity of a two-dimensional percolating medium, International Journal of Engineering Science 58 (2012) 78–84.

[18] N. Shashidhar, A. Shenoy, On using micromechanical models to describe dynamic mechanical behavior of asphalt mastics, Mechanics of Materials 34 (10) (2002) 657–669.

[19] R. Christensen, K. Lo, Solutions for effective shear properties in three phase sphere and cylinder models, Journal of the Mechanics and Physics of Solids 27 (4) (1979) 315–330.

[20] A. Aharony, D. Stauffer, Introduction to percolation theory, Taylor & Francis, 2003.

[21] D. Pham, T. Nguyen, Polarization approximations for macroscopic conductivity of isotropic multicomponent materials, International Journal of Engineering Science 97 (2015) 26–39.

[22] A. Tran, D. Pham, Polarization approximations for the macroscopic elastic constants of transversely isotropic multicomponent unidirectional fiber composites, Journal of Composite Materials 49 (30) (2015) 3765–3780.

[23] S.-T. Nguyen, D.-C. Pham, M.-N. Vu, Q.-D. To, On the effective transport properties of heterogeneous materials, International Journal of Engineering Science 104 (2016) 75–86.

[24] J. J. Timothy, G. Meschke, A cascade continuum micromechanics model for the effective elastic properties of porous materials, International Journal of Solids and Structures 83 (2016) 1–12.

[25] B.-V. Tran, D.-C. Pham, Refined polarization approximations for conductivity of isotropic composites, International Journal of Thermal Sciences 131 (2018) 72–79.

[26] B.-V. Tran, D.-C. Pham, M.-D. Loc, M.-C. Le, An adaptive approach for the chloride diffusivity of cement-based materials, Computers and Concrete 23 (2) (2019) 145–153.

[27] Z. Hashin, The elastic moduli of heterogeneous materials, Journal of Applied Mechanics 29 (1962) 143–150.

[28] C. Stolz, A. Zaoui, Analyse morphologique et approches variationnelles du comportement d'un milieu élastique hétérogène, Comptes rendus de l'Académie des sciences. Série 2, Mécanique, Physique, Chimie, Sciences de l'univers, Sciences de la Terre 312 (3) (1991) 143–150.

[29] M. Bornert, C. Stolz, A. Zaoui, Morphologically representative pattern-based bounding in elasticity, Journal of the Mechanics and Physics of Solids 44 (3) (1996) 307–331.

[30] L. Bardella, F. Genna, On the elastic behavior of syntactic foams, International Journal of Solids and Structures 38 (40-41) (2001) 7235–7260. doi:10.1016/S0020-7683(00)00228-6.
URL https://linkinghub.elsevier.com/retrieve/pii/S0020768300002286

[31] E. Hervé-Luanco, Simplification of the (n+1)-phase model and its extension to non linear behavior, International Journal of Solids and Structures 121 (2017) 135–147. doi:10.1016/j.ijsolstr.2017.05.021.
URL http://www.sciencedirect.com/science/article/pii/S0020768317302317

[32] J. Blondel, S. Joannès, E. Hervé-Luanco, Analytical modelling of the effect of morphological fluctuations on the transverse elastic behaviour of unidirectional fibre reinforced composites, International Journal of Solids and Structures (Aug. 2020). doi:10.1016/j.ijsolstr.2020.06.001.
URL http://www.sciencedirect.com/science/article/pii/S0020768320302213

[33] V. Marcadon, E. Herve, A. Zaoui, Micromechanical modeling of packing and size effects in particulate composites, International Journal of Solids and Structures 44 (25-26) (2007) 8213–8228.

[34] S. Torquato, Mean nearest-neighbor distance in random packings of hard d-dimensional spheres, Physical review letters 74 (12) (1995) 2156.

[35] M. Majewski, M. Kursa, P. Holobut, K. Kowalczyk-Gajewska, Micromechanical and numerical analysis of packing and size effects in elastic particulate composites, Composites Part B: Engineering 124 (2017) 158–174.

[36] M. Majewski, M. Wichrowski, P. Hołobut, K. Kowalczyk-Gajewska, Shape and packing effects in particulate composites: micromechanical modelling and numerical verification, Archives of Civil and Mechanical Engineering 22 (2) (2022) 86.

[37] M. Majewski, P. Holobut, M. Kursa, K. Kowalczyk-Gajewska, Packing and size effects in elastic-plastic particulate composites: Micromechanical modelling and numerical verification, International Journal of Engineering Science 151 (2020) 103271. doi:https://doi.org/10.1016/j.ijengsci.2020.103271.
URL https://www.sciencedirect.com/science/article/pii/S0020722520300598

[38] B. V. Tran, D. C. Pham, T. H. G. Nguyen, Equivalent-inclusion approach and effective medium approximations for elastic moduli of compound-inclusion composites, Archive of Applied Mechanics 85 (12) (2015) 1983–1995.

[39] F. De Larrard, Concrete mixture proportioning: a scientific approach, CRC Press, 1999.

[40] B. Bournonville, P. Coussot, X. Chateau, Modification du modèle de farris pour la prise en compte des interactions géométriques d'un mélange polydisperse de particules, Rhéologie 7 (2004) 1–8.

[41] R. Le Roy, E. Parant, C. Boulay, Taking into account the inclusions' size in lightweight concrete compressive strength prediction, Cement and concrete research 35 (4) (2005) 770–775.

[42] K. Miled, K. Sab, R. Le Roy, Particle size effect on eps lightweight concrete compressive strength: experimental investigation and modelling, Mechanics of Materials 39 (3) (2007) 222–240.

[43] K. Miled, K. Sab, R. Le Roy, Effective elastic properties of porous materials: Homogenization schemes vs experimental data, Mechanics Research Communications 38 (2) (2011) 131–135.

[44] R. Coble, W. Kingery, Effect of porosity on physical properties of sintered alumina, Journal of the American Ceramic Society 39 (11) (1956) 377–385.

[45] A. P. Roberts, E. J. Garboczi, Elastic properties of model porous ceramics, Journal of the American Ceramic Society 83 (12) (2000) 3041–3048.

[46] J. C. Smith, Experimental values for the elastic constants of a particulate-filled glassy polymer, J. Res. NBS 80 (1976) 45–49.

[47] J. Segurado, J. Llorca, A numerical approximation to the elastic properties of sphere-reinforced composites, Journal of the Mechanics and Physics of Solids 50 (10) (2002) 2107–2121. doi:10.1016/S0022-5096(02)00021-2.
URL https://linkinghub.elsevier.com/retrieve/pii/S0022509602000212

[48] L. Bardella, A. Sfreddo, C. Ventura, M. Porfiri, N. Gupta, A critical evaluation of micromechanical models for syntactic foams, Mechanics of Materials 50 (2012) 53–69. doi:https://doi.org/10.1016/j.mechmat.2012.02.008.
URL https://www.sciencedirect.com/science/article/pii/S0167663612000579

[49] A. A. Gusev, Controlled accuracy finite element estimates for the effective stiffness of composites with spherical inclusions, International Journal of Solids and Structures 80 (2016) 227–236. doi:10.1016/j.ijsolstr.2015.11.006.
URL https://www.sciencedirect.com/science/article/pii/S0020768315004680

[50] F. de Francqueville, P. Gilormini, J. Diani, Representative volume elements for the simulation of isotropic composites highly filled with monosized spheres, International Journal of Solids and Structures 158 (2019) 277–286. doi:10.1016/j.ijsolstr.2018.09.013.
URL https://www.sciencedirect.com/science/article/pii/S002076831830369X

[51] E. Ghossein, M. Lévesque, A fully automated numerical tool for a comprehensive validation of homogenization models and its application to spherical particles reinforced composites, International Journal of Solids and Structures 49 (11) (2012) 1387–1398. doi:10.1016/j.ijsolstr.2012.02.021.
URL https://www.sciencedirect.com/science/article/pii/S0020768312000613

[52] G. Tandon, G. Weng, Average stress in the matrix and effective moduli of randomly oriented composites, Composites science and technology 27 (2) (1986) 111–132. doi:10.1016/0266-3538(86)90067-9.

[53] D. C. Pham, Weighted effective medium approximations for conductivity of random composites, International Journal of Heat and Mass Transfer 51 (13) (2008) 3355–3361.

[54] B.-V. Tran, A simple model to predict effective conductivity of multicomponent matrix-based composite materials with high volume concentration of particles, Composites Part B: Engineering (2019) 106997.

[55] J. G. Berryman, Long-wavelength propagation in composite elastic media ii. ellipsoidal inclusions, The Journal of the Acoustical Society of America 68 (6) (1980) 1820–1831.

[56] X. Chateau, G. Ovarlez, K. L. Trung, Homogenization approach to the behavior of suspensions of noncolloidal particles in yield stress fluids, Journal of Rheology 52 (2) (2008) 489–506.

[57] L. Bardella, G. Perini, A. Panteghini, N. Tessier, N. Gupta, M. Porfiri, Failure of glass-microballoons/thermoset-matrix syntactic foams subject to hydrostatic loading, European Journal of Mechanics - A/Solids 70 (2018) 58–74. doi:10.1016/j.euromechsol.

2018.01.007.
URL https://linkinghub.elsevier.com/retrieve/pii/S0997753817308094